Understanding the Photomagnetic Behavior in Copper Octacyanomolybdates

ARTICLE *in* THE JOURNAL OF PHYSICAL CHEMISTRY A · AUGUST 2012

Impact Factor: 2.69 · DOI: 10.1021/jp303716z · Source: PubMed

8 AUTHORS, INCLUDING:

Oana Bunău
Xenocs
24 PUBLICATIONS **170** CITATIONS
SEE PROFILE

Philippe Sainctavit
French National Centre for Scientific Research
84 PUBLICATIONS **2,030** CITATIONS
SEE PROFILE

Amélie Juhin
French National Centre for Scientific Research
30 PUBLICATIONS **412** CITATIONS
SEE PROFILE

Valerie Marvaud
Pierre and Marie Curie University - Paris 6
62 PUBLICATIONS **1,843** CITATIONS
SEE PROFILE

Understanding photomagnetic behaviour in copper octacyanomolybdates

O. Bunău,[*,†] M.-A. Arrio,[†] Ph. Sainctavit,[†] L. Paulatto,[†] M. Calandra,[†] A. Juhin,[†] V. Marvaud,[‡] and C. Cartier dit Moulin[‡]

IMPMC, CNRS/UPMC, 4 place Jussieu, 75252 Paris, France , and IPCM, CNRS/UPMC, 4 place Jussieu, 75252 Paris, France

E-mail: bunau@impmc.upmc.fr

[*]To whom correspondence should be addressed
[†]IMPMC, CNRS/UPMC, 4 place Jussieu, 75252 Paris, France
[‡]IPCM, CNRS/UPMC, 4 place Jussieu, 75252 Paris, France

Abstract

The mechanism of photomagnetism in copper octacyanomolybdate molecules is currently under debate. Contrary to the general belief that the photomagnetic transition occurs only due to a photoinduced electron transfer from the molybdenum to the copper atom, recent X-ray magnetic dichroic (XMCD) data clearly indicate that this phenomenon is associated at low temperature to a local low spin - high spin transition on the molybdenum atom. In this article we provide theoretical justification for these experimental facts. We show the first simulation of X-ray absorption (XAS) and magnetic circular dichroism (XMCD) spectra at the $L_{2,3}$ edges of molybdenum, from the joint perspective of DFT calculations and Ligand Field Multiplet (LFM) theory. The description of electronic interactions seems mandatory for reproducing the photomagnetic state.

Introduction

Photomagnetic materials trigger an increased interest due to their potential applications as memory devices or optical switches.[1] Photoinduced magnetization of Prussian blue analogues was first observed in tri-dimensional networks.[2] Nowadays, technological studies have focused on the emerging trend towards miniaturization with a specific attention to smart photomagnetic species. Most of these new photomagnetic materials are based on switchable molecular units. In this context, researchers concentrate their efforts to design and synthesize nanostructured storage devices, engineered at the molecular scale.

Several classes of photomagnetic networks of Prussian blue analogues have been intensively studied.[3] In this work we will focus on molecules derived from octacyanomolybdates, one of the most recent synthesised networks.[4] In particular, we are interested in depicting the mechanism of photomagnetism in ($Mo(CN)_6(CN\text{-}CuL'_2)_2$) ($L'$ = for N,N',dimethyl ethylene diamine), labeled $MoCu_2$, seen as a prototype for a broader range of octacyanomolybdates compounds,[4,5] also containing $(Mo(CN)_2(CN\text{-}CuL)_6)^{8+}$ (L = tris(2-amino)ethylamine), labeled $MoCu_6$ and $Cs_2Cu_7(Mo(CN)_8))_4$. After photoexcitation with visible light ($\lambda = 406$ nm) for a few hours, the magnetic susceptibility

of $MoCu_2$ increases.[6] What renders these molecules so particular amongst other photomagnetic materials is the persistence of the photoinduced state up to room temperature. Several mechanisms explaining the photomagnetic transition in octacyanomolybdates have been proposed in the literature. In the first scenario, the transition is supposed similar to the one in bulk hexacyanoferrates Prussian blue analogues[1,2,7] and involves the charge transfer from Mo to Cu: Mo ($4d^2$) - Cu ($3d^9$) $\rightarrow$ Mo ($4d^1$) - Cu ($3d^{10}$).[3,4,8] The second hypothesis explains the magnetic metastable state through a local, low spin (S=0) - high spin (S=1) transition of the molybdenum atom.[5,6] Combined processes might also explain the photomagnetic properties.

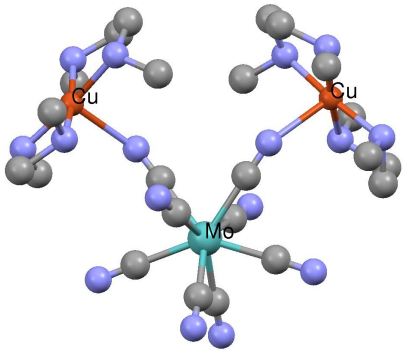

Figure 1: Central part of the motif for the MoCu2 molecule as determined from the diffraction pattern before photoexcitation. The metal ions are labeled. The two copper atoms are related by a C_2 axis traversing the molybdenum. Carbon atoms are in grey, nitrogen atoms in blue.

The only existing *ab initio* calculations on octacyanomolybdates focus on the $MoCu_6$ compound.[9,10] Post Hartree Fock calculations on a simplified structure,[10] used to investigate the nature of the photoinduced magnetic state, clearly dismiss the metal to metal charge transfer hypothesis and pick up the $d-d$ transition on the Mo^{IV} atom as the mechanism of photomagnetism. For these authors, the photomagnetic transition is accompanied by a change in the local structure as well as by the dissociation of a CN ligand.

The mechanism of the transition at low temperature can be depicted unambiguously by X-ray spectroscopy (XAS), which yields information on the electronic structure of the empty states. XAS is a very powerful tool in material science for its increased selectivity, both chemical (through the choice of the specific edge) and orbital (due to selection rules). Indeed, the $L_{2,3}$ edges of molyb-

denum probe directly the unoccupied *d* states and is sensitive to magnetic properties and to the geometrical environment of the absorbing atom. The available data have received various interpretations.[3,5,6] The X-ray magnetic circular dichroism (XMCD) is the difference in the absorption signal with circular right and left polarizations, respectively. Through the well established sum rules, XMCD yields important information about the ground state, concerning the number of holes in the valence band and the magnitude of spin and orbital magnetic moments. Some of us have performed XMCD measurements at the $L_{2,3}$ edges of molybdenum.[5,6] According to this study, the effective magnetic moments measured at 10 K were incompatible with the charge transfer scenario. Moreover, it was found that the number of holes on the molybdenum atom remains constant during the photomagnetic transition. It has therefore been proposed that a local spin transition centered on the molybdenum atom is responsible for the photomagnetic behaviour at low temperatures.[5,6] There is no experimental evidence for any charge transfer phenomena in the photomagnetic process at low temperature.

In this work we enforce this conclusion by presenting the first calculations of XAS and XMCD spectra on $MoCu_2$, seen as the prototype of MoCu systems. Calculations were compared with the experimental data from ref.[6] and provide interpretations of experimental spectra. The complex nature of these compounds required the use of complementary calculation methods. Indeed, the covalent nature of MoCu systems suggested the use of density functional theory (DFT) methods, whereas the spin degeneracy, essential for the description of XMCD data, prompted us to exploit the Ligand Field Multiplet theory. Only a few XAS theoretical studies containing one body and many body calculations on the same system exist,[11] albeit the obvious advantages and in our case the necessity of having a complementary vision on the material.

Our article is organized as follows. The next section contains the description of the molecule's structure, the motivation of our methodological approach as well as a brief description of the theoretical framewoks we have employed: the Ligand Field Multiplet theory and DFT calculations. In the following we show and discuss our results. Conclusions are presented in the last section.

About the calculations

Structure of the $MoCu_2$ molecule

The crystal structure of $MoCu_2$ belongs to the monoclinic space group C12/c1.[4] The conventional unit cell is base centered and contains 2×218 atoms (including hydrogen and water molecules), half of them being related to the other half by a fractional translation. The close environment of Mo in the formula unit is presented in Figure 1. To simplify calculations, we worked with the primitive unit cell, whose symmetry no longer relates to the one of the crystal but which comprises only half of the atoms (218). The primitive cell contains two formula units, hence the motif has 109 atoms.

The point group on the Mo site is C_2. A two-fold axis traverses the molybdenum atom, which is connected to eight CN ligands forming an intermediate structure between a dodecahedron and a square antiprism (Figure 1).

Methodology

XAS spectral shapes being similar at the L_2 and L_3 edges of Mo in $MoCu_2$, we decided to apply DFT methods in order to interpret experimental data. We worked in the framework of pseudopotentials, for both electronic structure and absorption cross section calculations.

In order to perform DFT calculations of XAS in MoCu systems, we recently developed the calculation of $L_{2,3}$ edges in the framework of pseudopotentials. The method was thoroughly tested and benchmarked. The details of the implementation are to be published elsewhere.[12]

For the ground state crystallographic data, we did not succeed to stabilize the magnetic Mo atoms. This very likely indicates that change of local structure may be needed for stabilizing the triplet ground state. These considerations, together with the fact that the spectral shapes of XMCD are slightly different at the L_2 and L_3 edges of Mo in $MoCu_2$,[13] prompted us to use a multi-electronic calculation method like the LFM theory. Both ground state and photomagnetic state were eventually calculated in the LFM framework.

Consequently, we show two complementary points of view on XAS at the $L_{2,3}$ edges of Mo before photoexcitation and point out explicitely the extent of their agreement.

Theoretical frameworks

The Ligand Field Multiplet theory

Ligand field multiplet theory (LFM) is an exact diagonalization technique of an atomic Hamiltonian, adapted to the calculation of X-ray absorption related spectroscopy. LFM is used extensively to describe the atomic-like excited states, as the $L_{2,3}$ edges in transition metal iono-covalent compounds or $M_{4,5}$ edges in rare earths. The theory and its practical implementation are due to the pioneering work of Theo Thole[14] and are based on the atomic calculations of R.D. Cowan[15] and on the group theory of P.H. Butler.[16] The absorption cross section is calculated according to the Golden Rule:

$$\sigma(\omega) = 4\pi^2\alpha\hbar\omega\frac{1}{d}\sum_{f,g}|\langle f|\vec{\varepsilon}\cdot\vec{r}|g\rangle|^2\delta\left(\hbar\omega - E_f + E_g\right) \quad (1)$$

Here $|g\rangle$ and $|f\rangle$ are the many body wavefunctions associated to the ground state configuration (no core hole) and to the excited one, respectively. The corresponding eigenvalues associated to these states are E_g and E_f, whereas d is the manifold of the ground state. The field operator $\vec{\varepsilon}\cdot\vec{r}$ is expressed in the electric dipole approximation, with $\vec{\varepsilon}$ the polarization and $\vec{r}$ the position vector. $\hbar\omega$ is the energy of the photon and α the fine structure constant. Transitions to s levels are found negligible and are not presented here. Consequently, at the $L_{2,3}$ edges of Mo^{IV} the initial and final state configurations write as $|g\rangle = |2p^6 4d^2>$ and $|f\rangle = |2p^5 4d^3>$, respectively. $|g\rangle$ and $|f\rangle$ are calculated through the diagonalization of the ground state and excited Hamiltonians. These Hamiltonians consist in a spherical part including the kinetic term, spin-orbit coupling, Coulomb electron-nucleon attraction and Coulomb electron-electron repulsion, which are calculated from a Hartree-Fock atomic model.[15] The Coulomb repulsion is scaled down by some adjustable factor in order to account for intra-atomic relaxation due to covalent effects. In particular, κ_{pd} et κ_{dd} are multiplicative factors, with respect to the atomic values, of the $p-d$ and $d-d$ Slater integrals

describing the electronic repulsions. The rotational invariance of the Hamiltonian is broken by two additional terms, the crystal field and the magnetic field interactions. The geometrical environment of the absorbing atom is taken into account through the crystal field, i.e. the electrostatic field of point charges whose disposure obeys the point group symmetry.[17]

In LFM calculations, the core hole lifetime is taken into account by convoluting with a Lorentzian function, with width of 1.8 eV for the L_3 edge and 2 eV for the L_2 edge.[18] Experimental convolution is accounted for *via* the convolution with a Gaussian having a width of 0.4 eV.[6]

DFT calculations

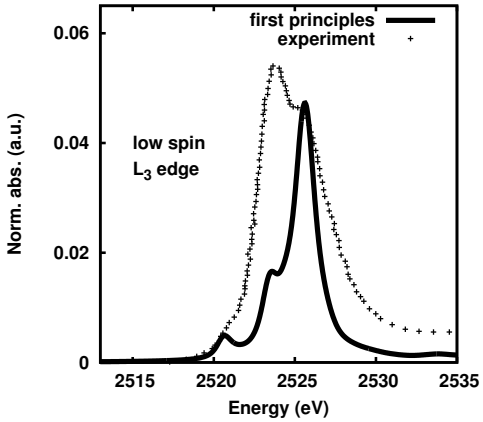

Figure 2: DFT calculations of the L_3 edge of Mo in $MoCu_2$. Experimental data is in dots, calculated isotropic XAS in solid line.

In the one body framework, the many electron wavefunctions $|f>$ and $|g>$ factorize into a (normalized) product of single particle orbitals. Consequently the cross section in (Eq. (1)) simplifies to:

$$\sigma(\omega) = 4\pi^2\alpha\hbar\omega\sum_{f,g}|\langle\Psi_f|\vec{\varepsilon}\cdot\vec{r}|\Psi_g\rangle|^2\delta\left(\hbar\omega-(E_f-E_g)\right) \tag{2}$$

where Ψ_g is the one particle wavefunction of the core level and Ψ_f the one of the probed, empty state. In our case $|\Psi_g\rangle$ corresponds to one of the six $j=1/2, m_j=\pm j$ and $j=3/2, m_j=-j,...,j$ and can be easily calculated by any atomic code. The difficult aspect is the calculation of the extended wavefunctions $|\Psi_f\rangle = |\Psi_d\rangle$ describing the d empty levels in the presence of the core

hole.

Reciprocal space, DFT plane waves calculations were performed with the Quantum Espresso package.[19] The electronic structure is calculated self-consistently with the PW program, by using pseudopotentials and periodic boundary conditions. On the top of the electronic structure calculation, the $L_{2,3}$ edges X-ray absorption cross section is obtained with the most recent version of the XSpectra program in the same package.[12] The absorption cross section is obtained through a Lanczos algorithm.[20,21] Spin orbit coupling on the 4*d* was neglected.

For electronic structure calculations we used a GGA description of exchange-correlation and a cut-off of 50 Ry and 500 Ry for the wavefunctions and charge density expansions, respectively. As a consequence of the size of the unit cell, a single k point (Γ) was enough to converge the DOS. The Fermi level is calculated self-consistently and used as the lower limit of the integral in Eq. (2). We used ultrasoft pseudopotentials, generated for the following atomic configurations: Mo $4s^2$ $5s^1$ $4p^6$ $5p^0$ $4d^5$, Cu $3d^{10}$ $4s^1$ $4p^1$, O $2s^2$ $2p^4$ $3d^2$, N $2s^2$ $2p^3$ $3d^0$, C $2s^2$ $2p^2$ $3d^2$ and H $1s^1$ $2p^1$. Spectra at the L_3 edge were convoluted with a Lorentzian function of 0.8 eV width to account for core hole lifetime and with a Gaussian of 0.4 eV width to acknowledge for the instrumental resolution.[6]

Results and discussion

DFT calculations

The agreement between the pseudopotential calculation of the L_3 edge of Mo in $MoCu_2$ and experimental data before photoexcitation is shown in Figure 2. The calculated Fermi level lies at 2520.5 eV, according to the experimental scale in Figure 2. Note that the convolution width is chosen small enough to reveal the three spectral structures. All peaks in the experimental spectrum have been reproduced at the correct relative energies, including the shoulder at 2521.5 eV. On the other hand, relative intensities of the two main peaks are not well reproduced. We are very confident in the accuracy of this DFT reciprocal space calculation, as similar results have been obtained by using the non-muffin tin real space calculation method in the FDMNES code[22,23] (not shown here,

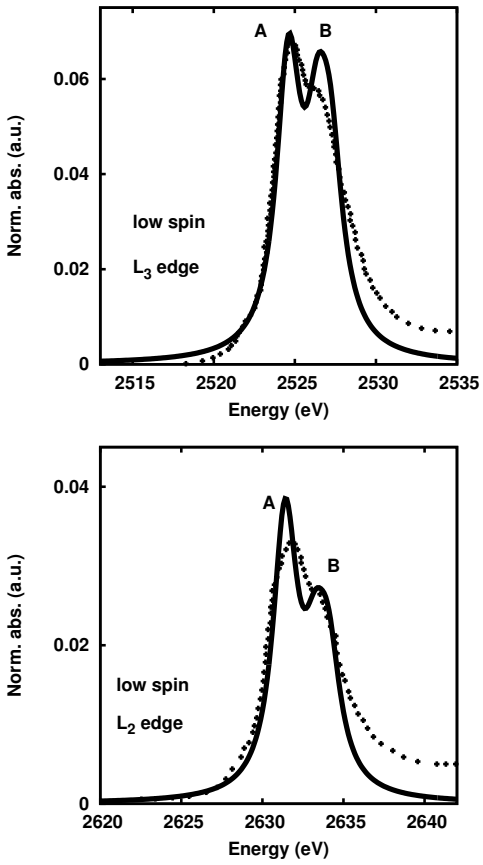

Figure 3: LFM calculations of the L_3 (above) and L_2 (below) edges in the low spin state of Mo^{IV} in a D_{4h} distorted environment. Experimental data is in dots, calculated isotropic XAS in thick solid.

for simplicity). Calculations with a fully screened hole on the $2p$ levels have not improved upon this issue. Although we do not have any confirmed explanation for the partial disagreement, we can speculate that its origin lies in the inappropriateness of description of the core hole in the DFT framework.

In the one body approximation and without spin-orbit coupling on the d states, the spectral shapes of L_3 and L_2 are the same, with the value for branching ratio rigorously equal to 2. We therefore chose not to show the XSpectra calculations at the Mo L_2 edge.

Note that the occupation number of the d band is 3.91, according to the occupancy of the atomic orbital $4d$ (Löwdin charges). This value is closer to the nominal charge of the neutral molybdenum atom ($n_d = 5$) then to the ionic charge indicated by the formal valence ($n_d = 2$ for Mo^{IV}). Since DFT in its local (LDA) and semilocal (GGA) approximations impedes the localization of the charge, it is not necessarily expected to reproduce formal charges in ionic compounds.

Ligand field multiplet calculations

We performed LFM calculations to reproduce the experimental spectra before and after photoexcitation. Taking into account the true symmetry on the molybdenum atom would suppose the use of four parameters to describe the crystal field. Since no experimental values for crystal field parameters are available, we decided to work in the more symmetric D_{4h} group, where only three structural parameters are needed. We fit the three parameters Ds, Dt and 10Dq accounting for the effective distortion.

The physics of MoCu systems, before and after photoexcitation, is captured through a convenient choice of parameters, as explained below. The best agreement with experimental data is shown in Figure 3 and Figure 4. All the experimental features in the XAS spectra were reproduced at the correct energy positions, at both L_2 and L_3 edges of Mo. In the following, the spectral structures will be referred to as peaks A, B and C (see Figure 3 and Figure 4). The theoretical spectrum for the low spin Mo has two main features (A and B) with an energy separation of ≈ 1.8 eV, comparable with the experimental findings. In the high spin case $L_{2,3}$ edges have three features, whose

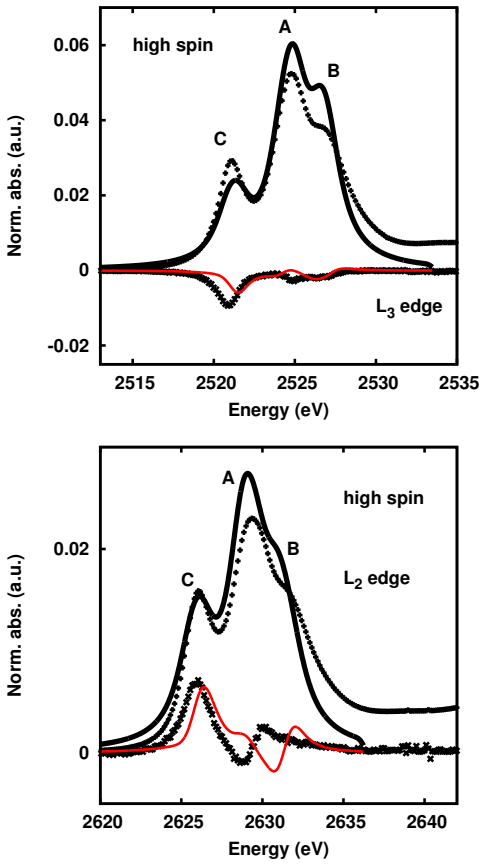

Figure 4: LFM calculations of the L_3 (above) and L_2 (below) edges of high spin Mo^{IV} in a D_{4h} distorted environment. Experimental data is in dots, calculated isotropic XAS (XMCD) in thick (thin) solid.

relative intensities are well reproduced by the calculations. It clearly appears that with the set of parameters that allow a fair simulation of XAS at both L_3 and L_2 edges, it is possible to compute an XMCD signal whose spectral shape is very similar to the experimental one. The LFM method calculates transitions from a $2p$ level to a $4d$ level so that transitions towards the continuum states with d symmetry are ignored. These transitions are responsible for the arctangent like step on the high energy side of the experimental spectra (Figure 3 and Figure 4).

The parameters are chosen along the strategy described in the following. In the low spin state, there exist several sets of parameters fitting the experimental data. Amongst these, we chose the one in closest agreement with our results issued from DFT calculations. In particular, we set electronic repulsions to zero, a limit that is close (but not identical) to the mean field approximation in the DFT framework. Indeed, in both cases, the energy separation between peaks A and B is due to the crystal field exclusively, while electronic levels are no longer split by repulsions. Furthermore, both LFM theory with zero Coulomb repulsions[13] and DFT mean-field theory predict an $L_{2,3}$ branching ratio of 2/3, in absence of spin-orbit coupling of the $4d$ levels. Under these circumstances, we guess that $k_{pd} = k_{dd} = 0$ is a natural choice in order to reproduce the spectra before photoexcitation. Structural (crystal field) parameters were optimized to the following values: 10Dq = -5.5 eV, Ds = -0.3 eV, Dt = -0.7 eV. In the low spin state (Figure 3), the ground state of Mo^{IV} is a spin singlet. The normalization of data is chosen as to yield the same integral of the experimental and calculated XAS spectra, after suppression of continuum states in the experimental data. Hence, both spectra are normalized to the same number of holes.

LFM calculations are essential to describe the high spin state, for two reasons. First, they allow to account for the change in local structure accompanying the photoexcitation. Indeed, DFT calculations suggested that some local distortion is involved with the photomagnetic state, however in the absence of structural data DFT calculations of the photoexcited state were not possible. Second, the description of electronic repulsion beyond mean field appears to be necessary in order to reproduce the XMCD data. We find that Coulomb $d-d$ repulsion is necessary in order to obtain the high spin state: the ground state in D_{4h} symmetry is a spin singlet for $k_{dd} = 0$. We equally

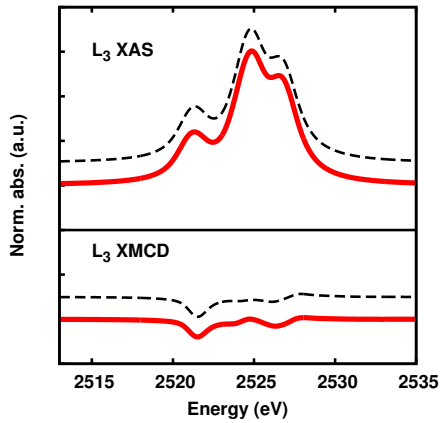

Figure 5: LFM calculations of XAS (upper panel) and XMCD (lower panel) at the L_3 edges of high spin Mo^{IV}: comparison between calculations with (thick solid) and without spin-orbit coupling on the 4d states (dashes). The two set of calculations were shifted vertically for visibility.

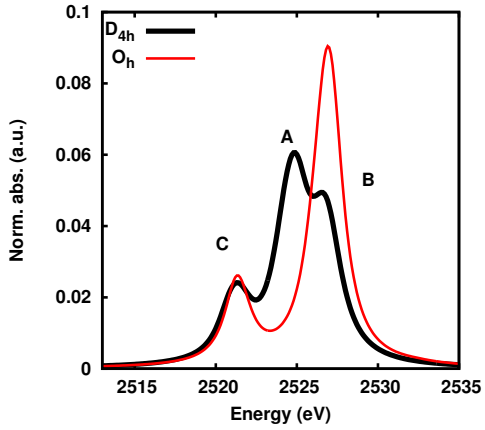

Figure 6: LFM calculations of XAS at the L_3 edges of high spin Mo^{IV}: comparison between the D_{4h} symmetry used to fit the experimental spectra (thick solid), and a calculation performed in O_h (thin solid) corresponding to the same 10Dq value (-5.5 eV). Calculations were shifted to fit the experimental energies.

find that the magnitude of Coulomb $p-d$ repulsions affects the shape of XMCD at A and B peaks energies. Consequently, in the high spin state, the optimized values of electronic repulsions are $\kappa_{pd} = 0.8$ and $\kappa_{dd} = 0.4$.

In the high spin state (Figure 4), the ground state of Mo^{IV} belongs to a spin triplet. The tetragonal distortion is now described by 10Dq = -5.5 eV, Ds = 0.4 eV and Dt = -0.2 eV. Calculations were performed for a temperature of 10 K and an external magnetic field of 6 Tesla, according to the experimental conditions.[6] We assumed that the Mo-Cu exchange coupling is negligible and thus the effective magnetic field on the Mo site is equal to the applied magnetic field.

$< S_z >=< g|S_z|g >$ and $< L_z >=< g|L_z|g >$ are the expectation values of the components of spin and orbit kinetic angular momenta along the direction of the magnetic field, in the initial configuration. In the low spin state $<S_z>$ is necessarily zero, whereas $|<L_z>| = 0.0015$ is negligible. In the high spin state, at T = 0, we found $< S_z >$ = -1 and $<L_z>$ = + 0.08. Note that the corresponding orbital magnetic moment $m_L = - < L_z > |\mu_B|$ and the spin magnetic moment $m_S = -g < S_z > |\mu_B|$ (g the gyromagnetic factor) have opposite directions. This is consistent with Hund's third rule since the $4d$ shell is less than half filled. At the experimental temperature T = 10 K, the two multiplet states $< S_z >$ = -1 and $< S_z >$ = 0 are populated, with weights 0.7 and 0.3 respectively, according to the Boltzmann statistics. Consequently, the magnetic moment of Mo at 10 K is equal to $\approx 1.4\ |\mu_B|$ (almost entirely due to the spin contribution), which is what one would expect from applying sum rules on the calculated spectrum and in close agreement with the value found in the experiment[6] (1.2 $|\mu_B|$).

We investigated the influence of the $4d$ spin-orbit coupling on the XAS and XMCD spectra and found it negligible (Figure 5). The absence of the $4d$ spin-orbit within DFT calculations appears to be a reasonable approximation.

Note the large value of 10Dq (-5.5 eV) needed to model the experimental data. For comparison, the value of 10Dq in iron cyanides (coordination number six) is $\approx$ 3 eV.[7] Crystal field on the $4d$ levels is larger than the one on the $3d$.[24] Indeed, it was found that in $SrMoO_3$ the 10Dq value for the crystal field on Mo site is 4 eV.[24] In the case of Mo cyanides the 10Dq value is expected to

be higher, as indicated by the spectrochemical series. Moreover, DFT XAS calculations of the ground state (Figure 2) suggest an approximate 10Dq of about 5eV, subject to some variations due to distortions. To obtain this value, we look at the energy difference between peak B and the feeble structure just above the Fermi level (2521 eV). It follows that value for the 10Dq parameter agrees to both DFT calculations and other similar LMF studies. Negative values of 10Dq are needed to account for the antiprism local structure. We verified that experimental data cannot be reproduced with 10Dq > 0, nor with Dt > 0.

Generally speaking, the distortion favours the singlet state, which is also visible in our particular choices of parameters. This is easily understood upon the fact that, in a cubic environment, Coulomb repulsion constrains each of the two d electrons to occupy one of the degenerated orbitals, hence to form a triplet state. When one gradually increases the distortion, from some point it will be more favorable energetically for the two electrons to occupy the same orbital than to overcome the barrier set by the crystal field and likewise populate two different orbitals. Hence, distortion and Coulomb repulsions compete into deciding the nature of the ground state: the former favours the singlet, whereas the latter favours the triplet.

We can associate peaks B and C with the O_h component of the crystal field, whereas peak A is a direct consequence of the distortion (see Figure 6). We found that peak A appears only for $|Dt|$ values above a certain threshold (0.2 eV in the high spin state, 0.5 eV in the low spin one). This means that experimental data (XAS, XMCD) for either the low spin nor the high spin state of Mo^{IV} cannot be reproduced in a perfect cubic symmetry. Through LFM calculations we confirm that the low spin state for two d electrons cannot be obtained in a cubic symmetry, even in the most favorable case when the Coulomb repulsion is set to zero.

Conclusions

We presented calculations of electronic structure and XAS at the $L_{2,3}$ edges of Mo in $MoCu_2$, from the joint perspective of DFT and LFM calculations. Within LFM, we reproduce satisfactorily XAS

and XMCD experimental data, before and after photoexcitation and point out the essential role of $d-d$ Coulomb interaction into stabilizing the high spin state at low temperature. On the other hand, the spin-orbit coupling on the $4d$ states has no significant effect. The crystal field parameter 10Dq is in good agreement with the DFT calculations, as well as with previously published values. Experimental data is in good agreement with the LFM results, which confirm that the low spin - high spin transition on the molybdenum atom is the mechanism responsible for the photomagnetic behaviour of copper octacyanomolybdates at low temperatures.

Acknowledgement

The authors would like to thank Delphine Cabaret and Yves Joly for fruitful discussions. Lise-Marie Chamoreau is thanked for having provided the structural data and for useful discussions. We acknowledge financial support from the SWITCH project of the ANR-BLANC-SIMI7-2010-0 program.

References

(1) Sato, O. *Journal of Photochemistry and Photobiology C - Photochemistry Reviews* **2004**, *5*, 203–223.

(2) Bleuzen, A.; Lomenech, C.; Escax, V.; Villain, F.; Varret, F.; Cartier dit Moulin, C.; Verdaguer, M. *Journal of the American Chemical Society* **2000**, *122*, 6648–6652.

(3) Bleuzen, A.; Marvaud, V.; Mathonière, C.; Siekluka, B.; Verdaguer, M. *Inorganic Chemistry* **2009**, *48*, 3453.

(4) Herrera, J. M.; Marvaud, V.; Verdaguer, M.; Marrot, J.; Kalisz, M.; Mathonière, C. *Angewandte Chemie* **2004**, *116*, 5584–5587.

(5) Brossard, S.; Volatron, F.; Lisnard, L.; Arrio, M.-A.; Catala, L.; Mathonière, C.; Mallah, T.;

Cartier dit Moulin, C.; Rogalev, A.; Wilhelm, F.; Smekhova, A.; Sainctavit, P. *Journal of the American Chemical Society* **2012**, *134*, 222–228.

(6) Arrio, M.-A.; Long, J.; Cartier dit Moulin, C.; Bachschmidt, A.; Marvaud, V.; Rogalev, A.; Mathonière, C.; Wilhelm, F.; Sainctavit, P. *The Journal of Physical Chemistry C* **2010**, *114*, 593–600.

(7) Cartier dit Moulin, C.; Villain, F.; Bleuzen, A.; Arrio, M.-A.; Sainctavit, P.; Lomenech, C.; Escax, V.; Baudelet, F.; Dartyge, E.; Gallet, J.-J.; Verdaguer, M. *Journal of the American Chemical Society* **2000**, *122*, 6653–6658.

(8) Ma, X.-D.; Yokoyama, T.; Hozumi, T.; Hashimoto, K.; Ohkoshi, S.-i. *Phys. Rev. B* **2005**, *72*, 094107.

(9) Carvajal, M.-A.; Reguero, M.; de Graaf, C. *Chem. Commun.* **2010**, *46*, .

(10) Carvajal, M.-A.; Caballol, R.; de Graaf, C. *Dalton Trans.* **2011**, *40*, .

(11) Juhin, A.; Brouder, C.; Arrio, M.-A.; Cabaret, D.; Sainctavit, P.; Balan, E.; Bordage, A.; Seitsonen, A. P.; Calas, G.; Eeckhout, S. G.; Glatzel, P. *Phys. Rev. B* **2008**, *78*, 195103.

(12) Bunau, O.; Calandra, M. *First principles calculations of $L_{2,3}$ X-ray absorption spectra in a PAW approach*, in preparation.

(13) Thole, B. T.; van der Laan, G. *Phys. Rev. A* **1988**, *38*, 1943–1947.

(14) Thole, B. T.; van der Laan, G.; Fuggle, J. C.; Sawatzky, G. A.; Karnatak, R. C.; Esteva, J.-M. *Phys. Rev. B* **1985**, *32*, 5107–5118.

(15) Cowan, R. *The Theory of Atomic Structure and Spectra*; Berkeley, University of California Press, 1981.

(16) Butler, P. *Point Symmetry Group Applications*; New York, Plenum Press, 1981.

(17) Lever, A.; Lascombe, J. *Inorganic Electronic Spectrosopy*; Elsevier, 1984.

(18) www.cxro.lbl.gov.

(19) Giannozzi, P. et al. *Journal of Physics: Condens. Matter* **2009**, *21*, 395502 (19pp).

(20) Taillefumier, M.; Cabaret, D.; Flank, A.-M.; Mauri, F. *Phys. Rev. B* **2002**, *66*, 195107.

(21) Gougoussis, C.; Calandra, M.; Seitsonen, A. P.; Mauri, F. *Phys. Rev. B* **2009**, *80*, 075102.

(22) Joly, Y. *Phys. Rev. B* **2001**, *63*, 125120–125129.

(23) Bunău, O.; Joly, Y. *J. Phys.: Condens. Matter* **2009**, *21*, 345501.

(24) Lee, Y. S.; Lee, J. S.; Noh, T. W.; Byun, D. Y.; Yoo, K. S.; Yamaura, K.; Takayama-Muromachi, E. *Phys. Rev. B* **2003**, *67*, 113101.

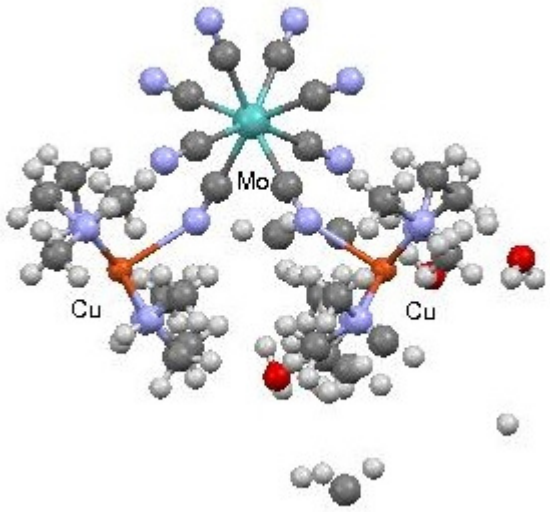
Mo
Cu
Cu